Embedded 3D vision system for automated micro-assembly

James Mure-Dubois and Heinz Hügli

University of Neuchâtel - Institute of Microtechnology, 2000 Neuchâtel, Switzerland

ABSTRACT

Machine vision plays an important role in automated assembly. However, present vision systems are not adequate for robot control in an assembly environment where individual components have sizes in the range of 1 to 100 micrometers, since current systems do not provide sufficient resolution in the whole workspace when they are fixed, and they are too bulky to be brought close enough to the components. A small-size 3D vision system is expected to provide two decisive advantages: high accuracy and high flexibility. The presented work aims to develop a 3D vision sensor easily embedded in a micro-assembly robot. The paper starts by a screening of 3D sensing methods, performed in order to identify the best candidates for miniaturization, and that results in the selection of the *multifocus* principle (which elegantly avoids the depth of field problem encountered for example in stereo vision). Here, depth is measured by determination of sharpness maxima in a stack of images acquired at different elevations. Then, it presents a preliminary system configuration, that delivers images of a 1300x1000 micrometers field of view with lateral resolution better than 5 micrometers and vertical resolution better than 20 micrometers. Finally, future steps in development of a real-time embedded multifocus sensor are presented, with a discussion of the most critical tradeoffs.

Keywords: 3D vision, micro-assembly, range imaging, automated assembly, depth from focus , micro vision, embedded vision, 3D sensing

1. INTRODUCTION

In automated micro-assembly, a robot is used to manipulate micro-sized parts. Accuracy requirements are such that assembly can not be realized through open-loop robot command. In order to close the loop, either for teleoperation[1,2] or autonomous[3,4] robot operation, vision sensors are used to provide feedback on the relative positions of the effector and parts to assemble. Most vision systems employed in automated micro-assembly are based on bulky microscopes[1,2,4,5,6] with a fixed field of view. Typically, such systems feature fixed robot effectors, centered within the microscope field of view. Parts are brought for assembly by a motorized stage moving under the microscope. This mode of operation is slow since a large mass must be set in motion for each new part introduced. In contrast with this approach, parallel robot systems (see figure 1) use low-mass effectors capable of being moved quickly over a large assembly workspace, allowing for much faster assembly. However, in this situation, a vision system covering all possible positions of the effectors (i.e. the whole assembly workspace) is not accurate enough. Therefore, for closed-loop operation, a high-resolution, embedded vision system must be considered. This approach has been used for example in planar assembly tasks[7], where a small camera provided vision feedback. For solving more general assembly tasks that require 3D vision, a universal 3D sensor is still missing. The presented work aims to develop a 3D vision sensor easily embedded in a micro-assembly robot. It is expected that 3D sensing will bring significant improvements for handling complex objects (free-form 3D objects with aspect ratio close to 1).

Section 2 introduces the main characteristics to consider in the design of an embedded, 3D vision sensor. Those characteristics are then used as guidelines in a screening of 3D measurement methods that could be deployed in a miniature sensor. Section 3 describes the 3D measurement principle we selected, while subsection 3.4 includes a discussion of some of its limitations with respect to miniaturization. In section 4, we present 3D measurements obtained with an experimental miniature imaging system, and compare the performance to a reference, high-resolution imaging system. Finally, section 5 provides a summary of the performance attained with a miniature multifocus system, together with a list of future developments required to realize a high performance 3D local vision sensor.

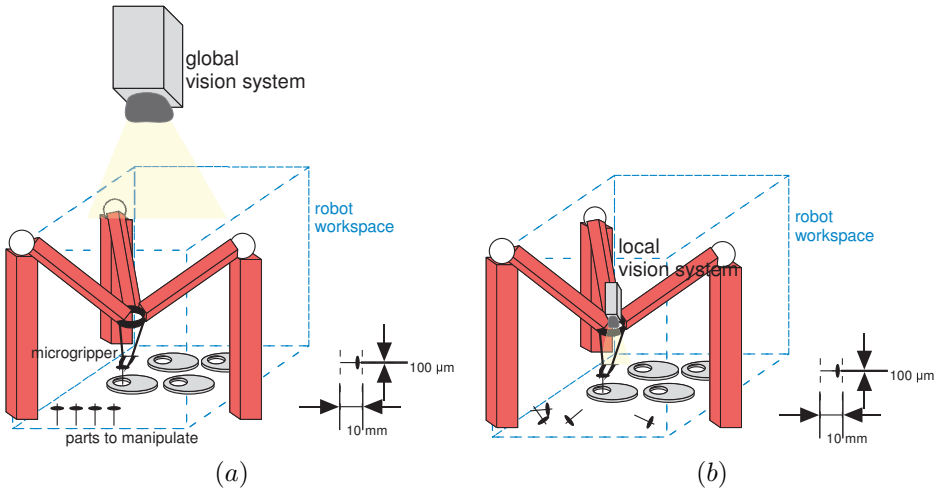

Figure 1. Micro-assembly robot with global (a) or embedded (b) vision systems.

2. EMBEDDED VISION SYSTEM REQUIREMENTS

In this section, we present a list of the desired properties for an embedded 3D vision sensor. The tradeoffs associated with each of these properties are also briefly discussed.

2.1. Mass

While sensor mass is generally not considered important in computer vision applications, it is, however, of key relevance for embedded system design. As a principle for a local sensor, the volume imaged is only a small fraction of the assembly workspace. This implies that the embedded sensor will be moved with the robot active systems (grippers, actuators) during assembly operations. Fast motion is possible only if sensor mass is low. As a guideline for a practical application, we set the constraint : $m \leq 100\,g$. We will see that this constraint is of critical importance, since it prohibits the use of high performance optics, such as bulky microscope objectives. This in turn limits the lateral and vertical resolution that can be attained. It also constrains the choice of the imager device (the pixel size must be small, in order to provide high resolution images with a small optical magnification).

2.2. Resolution - Field of view

In order to reach assembly tolerances, the spatial resolution (r_x, r_y, r_z) must be as high as possible. Furthermore, it is desirable to have a volume of view (L_x, L_y, L_z) as large as possible, in order to include all the relevant parts present in the workspace into the local 3D image. As a target for system design, we specify a range for the volume of view varying between $1\,mm^3$ and $1\,cm^3$. Since the number of pixels in a standard camera rarely exceeds 1000×1000, planar resolution will be, at best, limited to one thousandth of the volume of view $(0.1\,\mu m^{-1}, 0.1\,\mu m^{-1}) \leq (r_x, r_y) \leq (1\,\mu m^{-1}, 1\,\mu m^{-1})$. A compromise must be found between resolution and volume of view, depending on the target assembly application.

2.3. Frame rate

When used in a production environment, the 3D sensor must provide data in real-time. As a target value for a practical application, we specify that the data should be produced at $R = 10\,fps$ (allows real-time teleoperation, and more efficient autonomous operations). Depending on the final application, a lower frame-rate could be accepted, especially in applications where high-precision is more critical than high-speed operation.

2.4. Summary

The requirements exposed above are very different in their nature. It may show difficult to reach all target values simultaneously. Therefore, we need to set priority rules between the different requirements. Table 1 summarizes the expectations for a local 3D sensor, and exposes the main penalty if the expected values cannot be reached. When aiming for an embedded application, the highest priority shall be set to the compliance with the mass requirement. Next in order of priority comes the spatial resolution. Volume imaged and frame rate share the third level of priority.

Table 1. Expectations for local 3D vision sensor

Property	**Ideal case**	**Minimal expectation**	**Penalty**
Mass	As low as possible	$m \leq 100\,g$	Embedment in robot impossible
Spatial resolution	As high as possible	$r_x, r_y, r_z \geq 0.1\,\mu m^{-1}$	Assembly impossible (not accurate enough)
Volume imaged	As high as possible	$L_x, L_y, L_z \geq 1\,mm$	Not enough information (local scan required)
Frame rate	As high as possible	$R \geq 10\,fps$	Low assembly speed

2.5. Screening of depth measurement methods

The above criteria can be used as guidelines to select the most appropriate depth measurement principle for the design of an embedded 3D sensor. We will list here four approaches to 3D vision, and present the main elements to consider when aiming to develop a high resolution 3D imaging system. The goal here is not to discuss in depth all of these approaches, but to explain the selection of the multifocus method, which will be discussed in the next section. The approaches to 3D vision we considered are:

- Multifocus vision,
- White light interferometry,
- Depth from structured light,
- Depth from stereo.

In the multifocus approach[8,9], the object is imaged by a camera with a short depth of field. The camera is moved with respect to the object in order to perform a depth scan. Depth is determined by sharpness maximization algorithms applied to a stack of scanned images.
White light interferometry[10]involves two coherent light beams. The reference beam is reflected on a scan mirror, while the probe beam is projected on the object. Interference between the two reflected beams allow to measure the depth difference between object and reference mirror. Displacement of the scan mirror allows to obtain the range map for the entire object.
In depth from structured light[11,12], a high resolution light pattern is projected on the object, while the imaging device records the resulting image, which is characteristic of object topology. Software algorithms are used to determine the depth index encoded in the intensity structure recorded for each point. Depth is then obtained through triangulation.
Finally, in depth from stereo[13], the object is imaged by two cameras at different positions. By finding correspondences between the two images, depth can be computed through triangulation.
Of the four methods mentioned above, two require a mechanical depth scan (multifocus, white light interferometry), two require active illumination (white light interferometry, structured light), and one requires a correspondence matching algorithm (stereo vision). Some of the key characteristics of those methods are presented in table 2.

For an embedded implementation, depth from structured light and white light interferometry are ruled out by the mass requirements (mass of the active illumination setup). Stereo vision is limited by the resolution/depth

Table 2. 3D vision methods key characteristics

Method	Advantages	Penalties	Miniaturization issues
Multifocus	+ Passive system + Easy parametrization of z-resolution	- mechanical depth scan required - performance is sample dependent	- increased depth of field for miniature system - camera motion required
White light interferometry	+ high accuracy + low computational cost when using smart pixel sensors [14]	- mechanical scan required - limited depth range	- complex optics - active illumination required
Depth from structured light	+ low complexity processing + simple imaging hardware	- active illumination required - indexing problem	- light source miniaturization - indexing problem (occlusions)
Depth from stereo	+ passive system + no moving parts	- correspondence problem - small depth of view	- small depth of view

of field tradeoff : the high optical magnification required for high resolution imaging reduces the depth of field which, for stereo, limits the depth where correspondences can be found between image pairs. Contrasting with stereo, multifocus makes use of the limited depth of field when working at high magnification. This passive technique is therefore most appropriate when trying to produce high resolution 3D images. A more detailed description of this approach is given in the following section.

3. MULTIFOCUS 3D MICROSCOPY

In this section, we recall the basic principle of multifocus 3D measurements, present a simple model used for estimating its performance and finally, we give a brief theoretical overview of the limitations associated with miniaturization.

3.1. Depth measurement principle

The principle of multifocus 3D measurement is described in [15, 9]. A microscope with a short depth of field, is used to acquire a series of images $I_i(x, y)$ at different elevations z_i relative to the object (figure 2). After transformation of the images into associated sharpness images $S_i(x, y)$, the object depth for any pixel in the image is the depth associated to the image of maximum sharpness among the stack.

$$Z(x, y) = z_{\hat{i}(x,y)} \qquad \text{where} \quad \hat{i}(x, y) = argmax(S_i(x, y)) \tag{1}$$

The extent of the depth of field puts a higher limit to the achievable depth resolution.

3.2. Multifocus system key components

Based on the multifocus depth measurement principle presented above, we can distinguish 4 main components in a multifocus 3D imaging system:

- Optical component : image formation system.
- Electronic component : image sensor.
- Mechanical component : vertical translation mechanism (z-motor).
- Software component : control of camera displacement, sharpness maximization and depth determination algorithms.

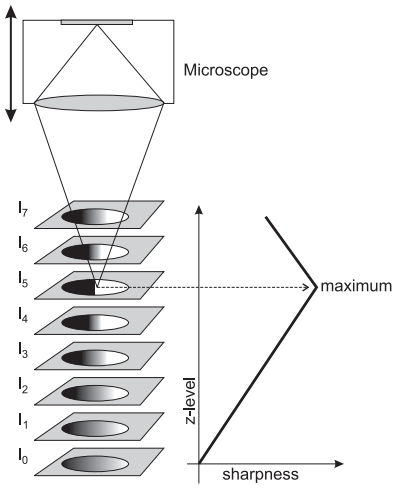

Figure 2. Multifocus 3D microscopy: measurement principle

The present work aims to analyze the effect of embedment constraints (principally mass) on the optical and electronic component, since those hardware components are the most critical with respect to 3D imaging performance. The topic of extending embedment compliance to the z-motor is left for a future work. Finally, we will list some perspectives for adaptation of software component to real-time constraints.

3.3. Multifocus software processing

The key element in multifocus software processing is sharpness analysis. The sharpness analysis is performed by applying an operator sensitive to high frequencies on the acquired intensity images. Among the various high-frequency sensitive operators, we used local variance[15] and Laplacian filters. For each image $I_i(x, y)$ in the stack, a sharpness map $S_i(x, y)$ is computed

$$S_i(x,y) = |I * K| \qquad \text{where K is for example a 5x5 Laplacian kernel} \quad K_5 = \begin{pmatrix} 1 & 2 & 3 & 2 & 1 \\ 2 & 4 & 8 & 4 & 2 \\ 3 & 8 & -84 & 8 & 3 \\ 2 & 4 & 8 & 4 & 2 \\ 1 & 2 & 3 & 2 & 1 \end{pmatrix} \tag{2}$$

A limitation of high frequency energy measurements such as described in equation 2 is sensitivity to noise. Therefore the dimension of sharpness operator kernels must be adapted to the scene measured (in order to probe spatial frequencies that are strongly represented in the scene). Even when the appropriate sharpness operator is used, presence of false depth readings caused by noise can not be avoided.

3.4. Multifocus with miniature imager

We have seen (section 2) that the mass requirement is the most critical in the development of an embedded 3D vision system. While a CCD sensor has very small mass, optics needed to form an image on the sensor are rather bulky; their weight can be minimized if :

- the lateral extent of the image is small
- the magnification is small

Therefore, an embedded vision system must use a small sensor, with minimal pixel pitch. The price to pay is a higher noise sensitivity for the sensor.

3.5. Theoretical expectations

The accuracy in depth determination will be at best of the same order of magnitude as depth of field. Depth of field is defined as the maximum displacement in depth for an object while its image blur stays confined within one pixel of the sensor. Using a simple, single lens model, depth of field DoF can be expressed[8] as :

$$DoF = \frac{2 \cdot \left(\frac{N_s \cdot \epsilon}{X} + 1\right) \cdot \epsilon \cdot f \cdot D}{D^2 \cdot \left(\frac{N_s \cdot \epsilon}{X}\right)^2 - \epsilon^2} \tag{3}$$

where:

- f is the focal length of the optical system,
- D is the optical system entrance pupil diameter,
- ϵ is the imaging sensor pixel pitch,
- N_s is the lateral extension of the sensor (in pixels),
- X is the lateral extension of the image field.

Note that the term $\frac{N_s \cdot \epsilon}{X}$ is simply the optical magnification M.
Equation 3 clearly shows that a short depth of field is obtained with short focal length, high magnification, and large entrance pupil diameter. For multifocus depth measurement, we are interested in having the shortest depth of field. But the entrance pupil diameter is limited by weight considerations in a local sensor. Similarly, reducing the focal length will reduce working distance for the sensor. The curve in figure 3 shows predicted depth of field a miniature imaging system when N_s, ϵ, D and f are fixed, and the optical magnification $M = \frac{N_s \cdot \epsilon}{X}$ is varied to accomodate for different object size into the field of view X. In this example, we chose $N_s = 752$, $\epsilon = 3\,\mu m$, $D = 7\,mm$, $f = 15\,mm$ (the values correspond to the experimental system of section 4), while the range for field dimension corresponds to the requirements in section 2. Three magnification values ($M = 0.3, 1.0, 3.0$) are reported on the curve.

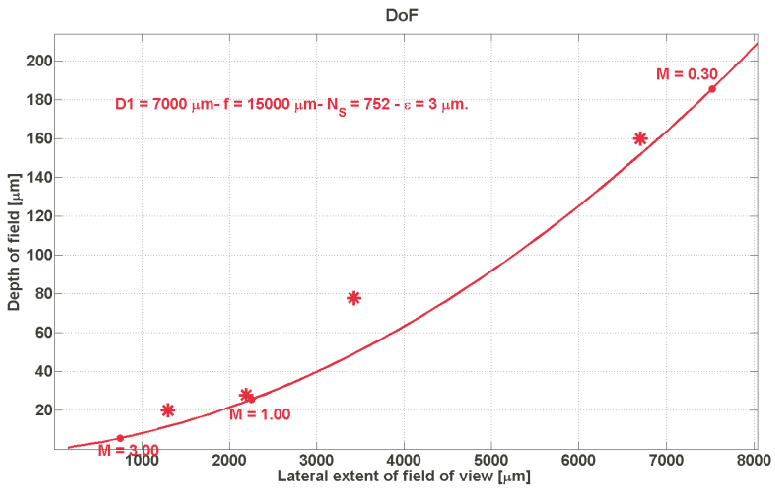

Figure 3. (Plain curve) Depth of field expectation for miniature imaging system - (Asterisks) Measured depth accuracy (see section 4.3)

Figure 4. Miniature imager with 15mm objective

3.5.1. Limitations of miniature multifocus system

Figure 3 indicates that the depth resolution for a multifocus system using a miniature imager is low when the field imaged is wide and it is high when the target field is narrow. For a $1 \times 1mm$ field, the depth of field is close to the minimal expectation for vertical accuracy defined in table 1 ($10\,\mu m$). Note that the depth of field is comparatively larger for miniature imagers, where the optical aperture is limited, when opposed to microscope systems.
Also, multifocus 3D is a passive method, which implies no illumination, and object dependent contrast. This limits the scope of applications to objects with sufficient contrast features. High accuracy is expected with some contrast rich metallic surfaces while uniform plastic surfaces provide much less accuracy.

4. EXPERIMENTAL RESULTS

4.1. Miniature system implementation

The implemented miniature imager uses a Kappa CH-166 micro-camera, that contains an 1/6" CCD sensor with PAL resolution (752×582). The pixel pitch is $\epsilon_x, \epsilon_y = 3.0\,\mu m \times 3.0\,\mu m$. Depending on the field to cover, different optical magnifications M must be employed. The camera objective has focal length $f = 15\,mm$, and spacer elements between objective and sensor allow to span magnifications ranging from $M = 0.25$ to $M \approx 2.0$. The micro-camera is shown on figure 4. The mass of the imager device (including objective) does not exceed $20\,g$. When compared to the expectations in table 1, this indicates that a mass budget of $80\,g$ can be spent on the z-motor in the development of the embedded system. Note that currently, our experimental setup uses much bulkier motors ($mass > 2\,kg$), since our purpose is to evaluate the miniature imager only.
The software component is realized as a C++ application on PC. This application controls camera displacement, image acquisition, sharpness maximization, noise filtering and display of range maps. Image acquisition is performed through a Matrox Meteor II frame-grabber. The sharpness evaluation algorithms are implemented either with MIL[16] or OpenCV[17], and sharpness maximization is performed in parallel with image stack acquisition. Nevertheless, sharpness determination remains a time consuming operation, especially when a large kernel is used (a typical processing time for an image (752×582) is $50\,ms$).

4.2. Sample images

We present depth maps acquired with the miniature imager system, which illustrate the adequacy of this component to the task proposed in section 1. The first sample is a detail of a screw viewed from top (figure 5), that was acquired at high magnification ($M = 1.85$). The dimensions of the scene $L_x \times L_y \times L_z$ are approximately $1300 \times 1000 \times 2500\mu m^3$. This example shows the potential of the miniature system to provide accurate depth data at high resolution, for high aspect ratio scenes. The 3D rendering allows to see that the system is able to measure the slope in the screw spirals. The second sample (figure 6) was acquired with low magnification ($M = 0.28$). The image shows a random arrangement of nails, which serves as an example of bulk part feeding

situation[3]. With range information, it is easy to distinguish the top nails from the bottom ones, so that an assembly robot can be programmed to automatically pick one of these parts for assembly.

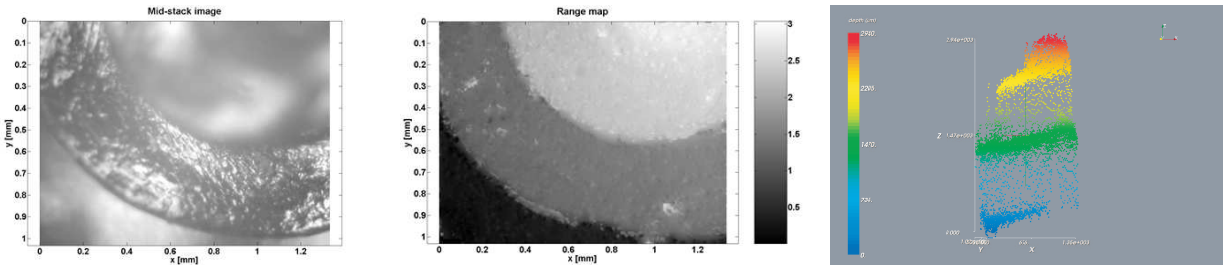

(*a*) Mid-stack image (*b*) Range image (*c*) 3D rendering

Figure 5. Sample image for miniature system : screw tip

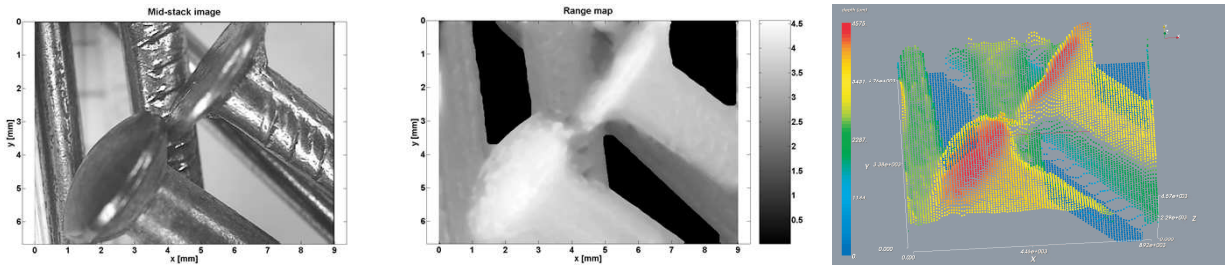

(*a*) Mid-stack image (*b*) Range image (*c*) 3D rendering

Figure 6. Sample image for miniature system : nails

4.3. Depth accuracy

Accuracy evaluation is difficult for passive 3D measurement systems, since range image quality depends on the image contents. To estimate depth accuracy, simple scenes (described by a simple geometric model) are measured. The scene used in our experiments, shown on figure 7 (a), features two identical disks, with diameter 19 mm. The height difference between the parts is $1.5 \pm 0.1\, mm$. This scene was imaged with different optical configurations (labels 1 to 4 in image 7 and table 3), resulting in different fields of view (see figure 7 (a)). For each test scene, the number of images in the stack was 128, the scanned depth range was $\Delta Z \approx 2\, mm$. The geometric model for each disk is a perfectly flat and horizontal surface. In each range map, two regions of interest (covering approximately one quarter of the image field) are selected: R_b (on the bottom disk) and R_t (on the top disk) . The accuracy is estimated as the range standard deviation σ, averaged for those two regions of interest :

$$\sigma = \frac{\sigma_l + \sigma_h}{2} \tag{4}$$

Measurement results are summarized in table 3, which also recalls accuracy values obtained with high-performance multifocus microscope systems [8], as reference values. Accuracy results for scenes 1 to 4 were also reported on

Table 3. Measurements with miniature imager (1 to 4), compared to accuracy obtained with microscope setups[8] (5, 6)

Scene	1	2	3	4	5	6
Imager	Miniature	Miniature	Miniature	Miniature	MZ12	DMLA
Field of view $[mm]$	6.7×5.1	3.4×2.6	2.2×1.7	1.3×1.0	0.9×0.9	0.3×0.3
Magnification	0.36	0.72	1.10	1.85	10.0	31.0
$\sigma[\mu m]$	160	78	28	20	5	2

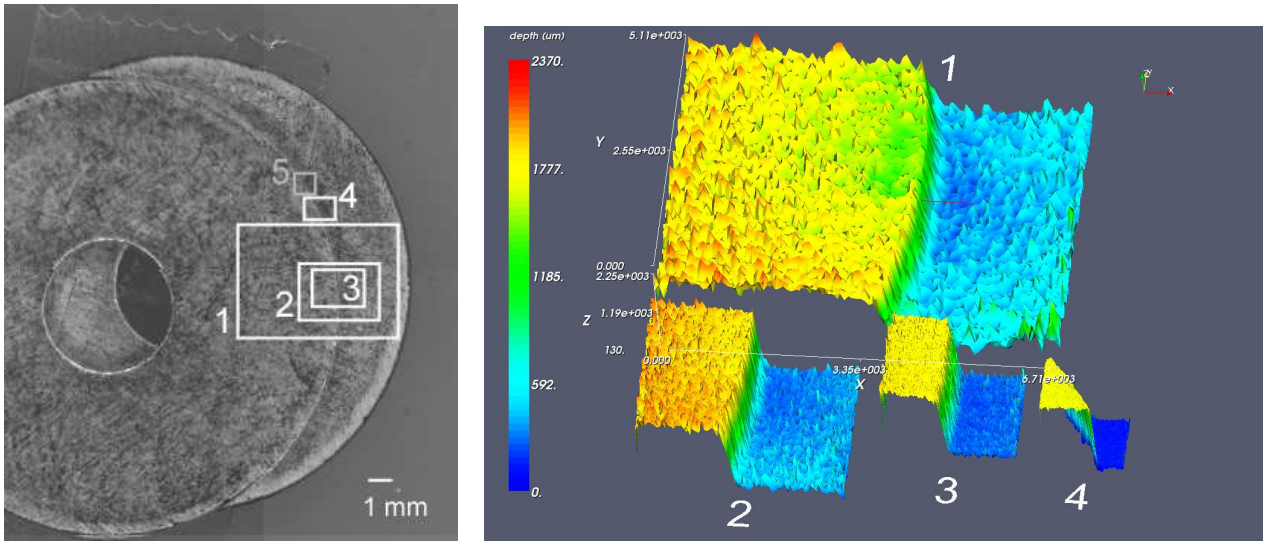

(a) (b)

Figure 7. Acccuracy measurement (Stacked metal disks) - (a) top view of the scene - (b) 3D rendering of measured range data for different fields of view (see table 3)

figure 3, where they can be compared to the depth of field values. As expected, the highest depth accuracy is obtained for narrowest field of view. The best accuracy obtained with our miniature imager is $20\,\mu m$. This result does not comply with the expectations of table 1 (a factor of 2 is missing). Figure 8 shows a comparison of test scenes acquired with miniature imager or microscope. A bulky microscope is 10 times more accurate (DMLA[8]). However, such a microscope is typically heavier than $3\,kg$. The observed 10-fold reduction in accuracy follows a 150-fold reduction in mass. Such a tradeoff is necessary if an embedded system is to be developped.

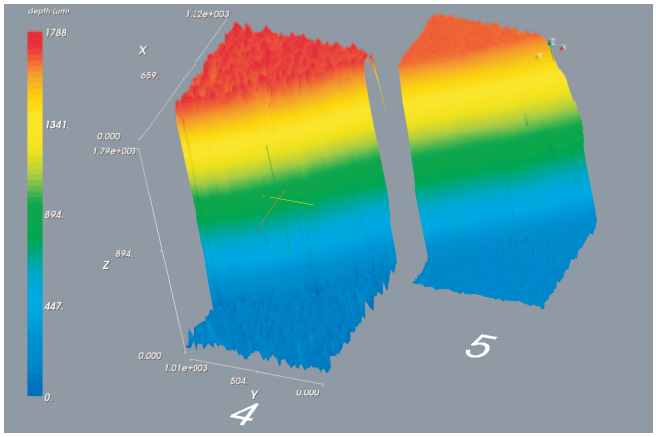

Figure 8. Range image acquired with miniature system (left) - Range image acquired with microscope system (right)

5. PERSPECTIVES

As mentioned above, the design of an embedded 3D vision sensor is far from complete. Many challenges remain if all expectations defined in table 1 are to be met. Table 4 summarizes the performance of the developped system and lists some perspectives for improvement in each area.

Table 4. Present performance of mutlifocus system, with perspectives for improvement.

Property	**Expectation**	**Current implementation**	**Improvement by**
Mass	$m \leq 100\,g$	$m > 2000\,g$ (imager : $20\,g$, motor : $2000\,g$	Low-mass z-motor
Spatial resolution	$r_x, r_y, r_z \geq 0.1\,\mu m^{-1}$	$r_x, r_y, r_z = 0.6 \times 0.6 \times 0.05\,\mu m^{-3}$	(Higher optical aperture)
Volume imaged	$L_x, L_y, L_z \geq 1\,mm$	$L_x, L_y, L_z = 1.3 \times 1.0 \times 3.0\,mm^3$	
Frame rate	$R \geq 10\,fps$	$R < 0.25\,fps$	Fast z-motor, fast camera, ROI processing, on-chip contrast processing

5.1. Low-mass multifocus motor

We have seen that multifocus with a miniature imager can reach accuracy specifications in the order of $20\,\mu m$, with a mass budget of $20\,g$ for the imager. The following step in development of an embedded multifocus sensor is the selection of an appropriate z-motor, capable of moving this $20\,g$ imager mass over a stroke of $5\,mm$ or more, while the motor mass stays under $80\,g$. This step is required for the completion of a first embedded 3D sensor prototype. Apart from mass, criteria to consider for motor selection are : linear accuracy, length of stroke, and speed of operation. For a first embedded prototype, mass and linear accuracy are considered critical, while length of stroke and speed of operation are secondary.

5.2. High-frame rate imaging

In order to meet the frame rate specification of table 1, additional steps are required. First, the z-motor must move the imager package with $10\,Hz$ period. Second, the image sensor must acquire images at a rate of $200\,fps$ (under the assumption that one range image requires a stack of 20 2D images). Finally, the software component must compute sharpness images at the same rate, i.e. in less than $5\,ms$. To reach this goal, sharpness determination could be performed on a small region of the image only (using a 200×200 region of interest allows to reduce the computation time by a factor higher than 10). Alternatively, smart imagers with on-chip processing could be used to speed up the computation of sharpness values.

6. CONCLUSION

This paper is a contribution to the development of a 3D vision system suited for a micro-assembly robot. The presented analysis of typical requirements shows that mass limitations are most critical. Mass considerations motivated the selection of the multifocus approach for depth determination. During the first step of development presented in this paper, a multifocus system using miniature image sensor and optical imaging system, but bulky z-motor, was realized, in order evaluate the performance of a miniature imager.
Experiment results showed that the depth accuracy for the system with miniature imager ($mass < 20\,g$) is close to $20\,\mu m$, which represents degradation in performance by a factor of about 10 when compared with a classical system based on a bulky microscope. The next step identified in the design of an embedded 3D sensor based on the multifocus approach is the integration of a low-mass z-motor. Finally, a fully functional embedded 3D sensor supposes real-time processing. Two possibilities are considered for this step: limitation of the field of view to a 200×200 region of interest, or on-chip processing for sharpness calculation by a dedicated imager.

ACKNOWLEDGMENTS

This work was realized in collaboration with Centre Suisse d'Electronique et de Microtechnique SA, Switzerland.

REFERENCES

1. T. Sulzmann, J. Carlier and J. Jacot, "Distributed microscopy: towards a 3D computer graphic-based multi user microscopic manipulation, imaging and measurement system.," in *Sensor Fusion and Distributed Robotic Agents*, P. Schenker and G. McKee, eds., *Proc. SPIE* **2905**, pp. 183–191, 1996.
2. A. Ferreira, J.-G. Fontaine and S. Hirai, "Automation of a teleoperated microassembly desktop station supervised by virtual reality," *Transactions on Control, Automation, and Systems Engineering* **4**(1), pp. 2519–2535, 2002.
3. R. Hollis and J. Gowdy, "Miniature Factories for Precision Assembly," in *International Workshop on Micro-Factories*, pp. 9–14, 1998.
4. R. Kallio, Q. Zhou, J. Korpinen and H. Koivo, "Three Dimensional Position Control of a Parralel Micromanipulator Using Visual Servoing," in *Microrobotics and Microassembly II*, B. J. Nelson and J.-M. Breguet, eds., *Proc. SPIE* **4194**, pp. 103–111, 2000.
5. S. Fatikow, J. Seyfried, S. Fahlbusch A. Buerkle and F. Schmoeckel, "A Flexible Microrobot-Based Microassembly Station," *Journal of Intelligent and Robotic Systems* **27**, pp. 135–169, 2000.
6. D.-H. Kim, K. Kim, K.-Y. Kim and S.-M. Cha, "Dexterous Teleoperation for Micro Parts Handling Based on Haptic/Visual Interface," in *2001 IEEE International Symposium on Micromechatronics and Human Science*, pp. 211–217, 2001.
7. J. Hesselbach and G. Pokar, "Assembly of a miniature linear actuator using vision feedback," in *Microrobotics and Microassembly II*, B. J. Nelson and J.-M. Breguet, eds., *Proc. SPIE* **4194**, pp. 13–20, 2000.
8. T. Zamofing and H. Hügli, "Applied multifocus 3D microscopy," in *Two- and Three-Dimensional Vision Systems for Inspection, Control, and Metrology.*, B. G. Batchelor and H. Hügli, eds., *Proc. SPIE* **5265**, pp. 134–144, 2004.
9. P. Geissler and T. Dierig, *Depth-from-Focus*, Handbook of Computer Vision and Applications, San Diego Academic Press, 1999.
10. P.H. Tomlins and R.K. Wang, "Theory, developments and applications of optical coherence tomography," *J. Phys. D: Appl. Phys.* **38**, pp. 2519–2535, 2005.
11. L.-S. Bieri and J. Jacot, "Three dimensionnal vision using structured light applied to quality control in production line," in *Optical Metrology in Production Engineering*, M. T. W. Osten, ed., *Proc. SPIE* **5457**, pp. 463–471, 2004.
12. T.Ha, Y. Takaya, T.Miyoshi, S. Ishizuka and T. Suzuki, "High-precision on-machine 3d shape measurement using hypersurface calibration method," in *Machine Vision and its Optomechatronic Applications*, H. C. S. Kaneko, ed., *Proc. SPIE* **5603**, pp. 40–50, 2004.
13. G. Danuzer, "Stereo light microscope calibration for 3d submicron vision," in *Proceeding of the 18th ISPRS Congress*, **31/B5**, pp. 101–108, (Vienna, Austria), July 1996.
14. Heliotis AG, "Heliotis real-time 3D imaging," 2005. URL http://www.heliotis.ch/.
15. John E. Ens, *An investigation of methods for determining depth from focus.* PhD thesis, University of British Columbia, 1990.
16. Matrox, "MIL: Matrox Imaging Library." URL http://www.matrox.com/.
17. Intel Corporation, "Open Source Computer Vision Library." URL http://www.intel.com/technology/computing/opencv/index.